Journal of Cellular Biochemistry 100:527–543 (2007)

Genetic Network and Pathway Analysis of Differentially Expressed Proteins During Critical Cellular Events in Fracture Repair

Xinmin Li,[1,2] Hali Wang,[3] Edward Touma,[2] Emma Rousseau,[4] Richard J. Quigg,[2,5] and James T. Ryaby[4]*

[1]College of Animal Science & Technology, Shanxi Agricutural University, Taigu, Shanxi 030801, People's Republic of China
[2]Functional Genomics Facility, Division of Biological Science, The University of Chicago, Chicago, Illinois 60637
[3]Zimmer, Inc., 12024 Vista Parke Dr., Austin, Texas 78726
[4]Research and Development, OrthoLogic Corp, Tempe, Arizona 85281
[5]Department of Medicine, Division of Biological Sciences, The University of Chicago, Chicago, Illinois 60637

Abstract Bone repair consists of inflammation, intramembranous ossification, chondrogenesis, endochondral ossification, and remodeling. To better understand the translational regulation of these distinct but interrelated cellular events, we used the second generation of BD Clontech™ Antibody Microarray to dissect and functionally characterize proteins differentially expressed between intact and fractured rat femur at each of these cellular events. Genetic network analysis showed that proteins differentially expressed within a given cellular event tend to be physically or functionally correlated. Seventeen such interacting networks were established over five cellular events that were most frequently associated with cell cycle, cell death, cell-to-cell signaling and interaction, and cell growth and proliferation. Eighteen molecular pathways were significantly enriched during the bone repair process, of which ERK/MAPK, NF-kB, PDGF, and T-cell receptor signaling pathways were significant during three or more cellular events. The analyses revealed dynamic temporal expression patterns and cellular-event-specific functions. The inflammation event on Day 1 was characteristic of the cell cycle-related molecular changes. The relative quiet stage of intramembranous ossification on Day 4 and the molecularly most active stage of chondrogenesis on Day 7 were featured by coordinated cell death and cell-proliferation signals. Endochondral ossification on Day 14 experienced a clear transition from the molecular/cellular function to the physiological system development/function. The osteoclast-mediated remodeling on Day 28 was highlighted by the integrin signaling pathway. The distinct changes in protein expression during these cellular events provide a molecular basis for developing cellular event-targeted therapeutic strategy to accelerate bone healing. J. Cell. Biochem. 100: 527–543, 2007.

Key words: protein expression profile; pathway analysis; bone repair; rat

Bone repair is a complex biological process and is marked by the critical cellular events of inflammation, intramembranous ossification, chondrogenesis, endochondral ossification, and remodeling [Jingushi et al., 1992; Hadjiargyrou et al., 2002]. The central theme of bone-repair biology is to understand molecular signals that trigger these highly coordinated cellular events, events that are regulated both transcriptionally and translationally.

Previous studies on molecular mechanisms of bone repair have primarily focused on transcriptional regulation, with the vast majority of those studies concentrating on the expression of specific genes [Bostrom and Asnis, 1998; Rosier et al., 1998; French et al., 2004]. Several landmark studies have recently been conducted utilizing microarray technology to reveal the

Grant sponsor: OrthoLogic Corp.; Grant sponsor: Division of Biological Sciences; Grant sponsor: Cancer Research Center; Grant sponsor: NIDDK Biotechnology Center, University of Chicago; Grant number: U24D55370.

*Correspondence to: James T. Ryaby, PhD, OrthoLogic Corp, 1275 W. Washington Street, Tempe, AZ 85281.
E-mail: jryaby@olgc.com

Received 6 October 2005; Accepted 4 June 2006
DOI 10.1002/jcb.21017

global expression profile, which has clearly demonstrated the biological complexity of bone repair [Hadjiargyrou et al., 2002; Hatano et al., 2004; Nakazawa et al., 2004; Li et al., 2005].

The use of microarrays for gene expression profiles has proven to be a powerful tool in elucidating the molecular basis of bone repair. However, protein synthesis and function are not a direct consequence of the RNA expression, and mRNA levels do not always correlate well with protein synthesis [Chen et al., 2002; Cutler, 2003]. It is, therefore, desirable to systematically study translational regulation during bone repair, which will complement mRNA profiling and provide verifiable assignment of gene function. Several attempts have been made to use protein antibody arrays for protein expression profiling in a complex biological process [Anderson et al., 2003; De Ceuninck et al., 2004; Hudelist et al., 2004; Ghobrial et al., 2005; Haab, 2005 for review]. Anderson et al. [2003] used the first generation of BD Clontech™ Antibody Microarray to look for differences in the expression patterns of primary muscle cultures from a type II spinal muscular atrophy patient (SMA) and a normal control. Three of the differentially expressed proteins were found to bind to p53, which interacts with the survival motor neuron (*SMN*) gene, the gene that is responsible for over 97% of SMA cases. These studies have established its feasibility and advantages. However, protein expression profiles during the bone healing have not been investigated using any of the protein array-based technologies.

In this study, we took advantage of the recently available second generation of BD Clontech™ Antibody Microarray, which includes over 500 monoclonal antibodies immobilized onto a glass slide, to simultaneously evaluate translational changes in the fractured rat femur on days 1, 4, 7, 14, and 28 relative to non-fractured controls. These time points were selected to represent times of key cellular events of the bone repair process. Our aim was to identify differentially expressed proteins coinciding with each of the key cellular events, and to reveal interacting networks and significantly enriched molecular pathways responsible for a given cellular event.

MATERIALS AND METHODS

Animals

Male Sprague–Dawley laboratory rats were obtained from Harlan (Indianapolis, IN) and housed at the research animal lab under conditions of 12 h light, 12 h darkness, ambient temperature of 20–23°C, and relative humidity of 35–60%. Experimental animal procedures were in compliance with animal welfare regulation and approved by the OrthoLogic Research Department.

Experimental Design and Tissue Collection

Ten-month-old male rats weighing from 400 to 500 g each were used in this study. Standard closed fractures of the right femur midshaft were created using the device and method as described by Bonnarens and Einhorn [1984]. The fractures were verified via contact radiograph using the Hewlett Packard Model #43855-A Faxitron Closed X-ray System. Before tissue collection, the rats were euthanized by intraperitoneal injection of 2 ml Euthasol (Delmarva Labs, Midlothian, VA). One centimeter of fractured femur, including early fracture callus and cortical bone shaft, from each group was harvested at five time points (Day 1, 4, 7, 14, and 28), and each time point had three replicates. In addition, three intact, age-matched rat femurs (three replicates) were used as controls (i.e., pin was not applied to and marrow was not removed from the control femurs). Fractured femurs were carefully dissected and cleaned to ensure no muscle contamination and midshafts were cut off using a sterile dremel saw blade and frozen in liquid nitrogen until protein extraction.

Protein Labeling and Antibody Array Hybridization

Protein extraction and labeling were performed using BD Clontech™ Protein Extraction & Labeling Kit. In brief, 150 mg of bone samples were thawed and homogenized in non-denaturing buffer (Clontech), and then diluted after the protein concentration had been measured with the BCA kit (Pierce, Rockford, IL). Each protein sample was labeled with Cy3 and Cy5 dye (Amersham) separately before being passed through a PD desalting column (Amersham). The Cy5- and Cy3-labeled proteins were then mixed and added to Antibody Microarray 500 array (A list of the antibodies on the Antibody Microarray 500 array can be found from the BD Clontech™ web site: http://bioinfo.clontech.com/abinfo/ab-list-action.do). The arrays were hybridized at room temperature for 30 min before a series of washes. The slide was dried

and scanned using a GenePix 4000B scanner (Axon Instruments). The initial quantification of array images was performed using GenePix Pro 6.0 software. Signal intensity for each protein was determined by averaging background-subtracted medium intensities from Cy3 and Cy5 channels.

It is noted that we modified the labeling methods to fit our experimental design (time series). Traditionally, to control for differences in labeling efficiency, samples A and B are each split into two equal portions. Each portion is then labeled with either Cy5 or Cy3 to produce four samples: A-Cy3, A-Cy5, B-Cy3, and B-Cy5. These four samples are combined to produce a mixture of Cy5- and Cy3-labeled proteins. A-Cy5 is combined with B-Cy3 (Mix1), while A-Cy3 is combined with B-Cy5 (Mix2). These mixes are then hybridized with the two Antibody Microarrays. One microarray is hybridized with Mix 1 and the second microarray is hybridized with Mix 2. In this set up, array 1 measures A-Cy5/B-Cy3 (Ratio 1) and array 2 measures B-Cy5/A-Cy3 (Ratio 2). Then, an internally normalized ratio (the square root of ratio1/ratio2) is calculated, which represents the abundance of an antigen in sample A relative to that of sample B. This design fits well with direct comparison of two samples and is not ideal for time series studies. Therefore, we adopted a different strategy for the sample labeling in this experiment. We split each sample into two equal portions, one labeled with Cy5 and other labeled with Cy3. Two labeled portions from the same sample were then combined, and hybridized to a single Antibody Microarray. The average signal intensity from Cy5 and Cy3 for each protein from each array was considered as raw data, which was used for subsequent data normalization and comparison analysis. This design of protein labeling can correct dye-dependent bias, and is also convenient for comparing samples across multiple time points

Data Analyses

Data normalization and comparison analyses were performed using GeneSpring 7.2 (Silicon Genetics). The data were normalized to median intensity (per chip) to allow relative comparisons between samples. The thresholds for selecting statistically differentially expressed proteins were set at a relative difference >1.5-fold, statistical difference at $P < 0.05$ (1-way ANOVA parametric test was performed assuming variances unequal). Using these thresholds, the false discovery rate (FDR) is $<5\%$ (we used median FDR, which was estimated by performing 720 permutations using dCHIP [Li and Wong, 2001]). We first identified differentially expressed proteins that met the above thresholds simultaneously at each time point relative to non-fracture controls; then, we dissected cellular-event-specific proteins (see Fig. 1 legend for details); finally, we used these cellular-event-specific proteins for Ingenuity Pathway Analysis as described below.

Global functional analyses, network analyses, and canonical pathway analyses were performed using Ingenuity Pathway Analysis 3.0 (Ingenuity® Systems, www.ingenuity.com). A differentially expressed gene list containing gene identifiers and corresponding fold changes was first uploaded as an Excel spreadsheet into the software. Each gene identifier was mapped to its corresponding gene object in the Ingenuity Pathways Knowledge Base. These genes were then used as the starting point for generating biological networks. The following is a brief description for each of the analyses (more detailed description can be found on the Ingenuity website: www.ingenuity.com).

Global functional analysis. Global functional analysis identified the biological functions that were most significant to the data set. Genes associated with biological functions in the Ingenuity Pathways Knowledge Base were considered for the analysis. The biological functions assigned to the analysis were first ranked according to the significance of that biological function to the analysis. Fischer's exact test was used to calculate a *P*-value determining the probability that each biological function assigned to that data set is due to chance alone.

Network analyses. Each gene identifier was mapped to its corresponding gene object in the Ingenuity Pathways Knowledge Base. These genes, called focus genes that served as the "seeds" for generating networks, were overlaid onto a global molecular network developed from information contained in the Ingenuity Pathways Knowledge Base. Networks of these focus genes were then algorithmically generated based on their connectivity. The network was a graphical representation of the molecular relationships between genes/gene products. Genes or gene products were represented as

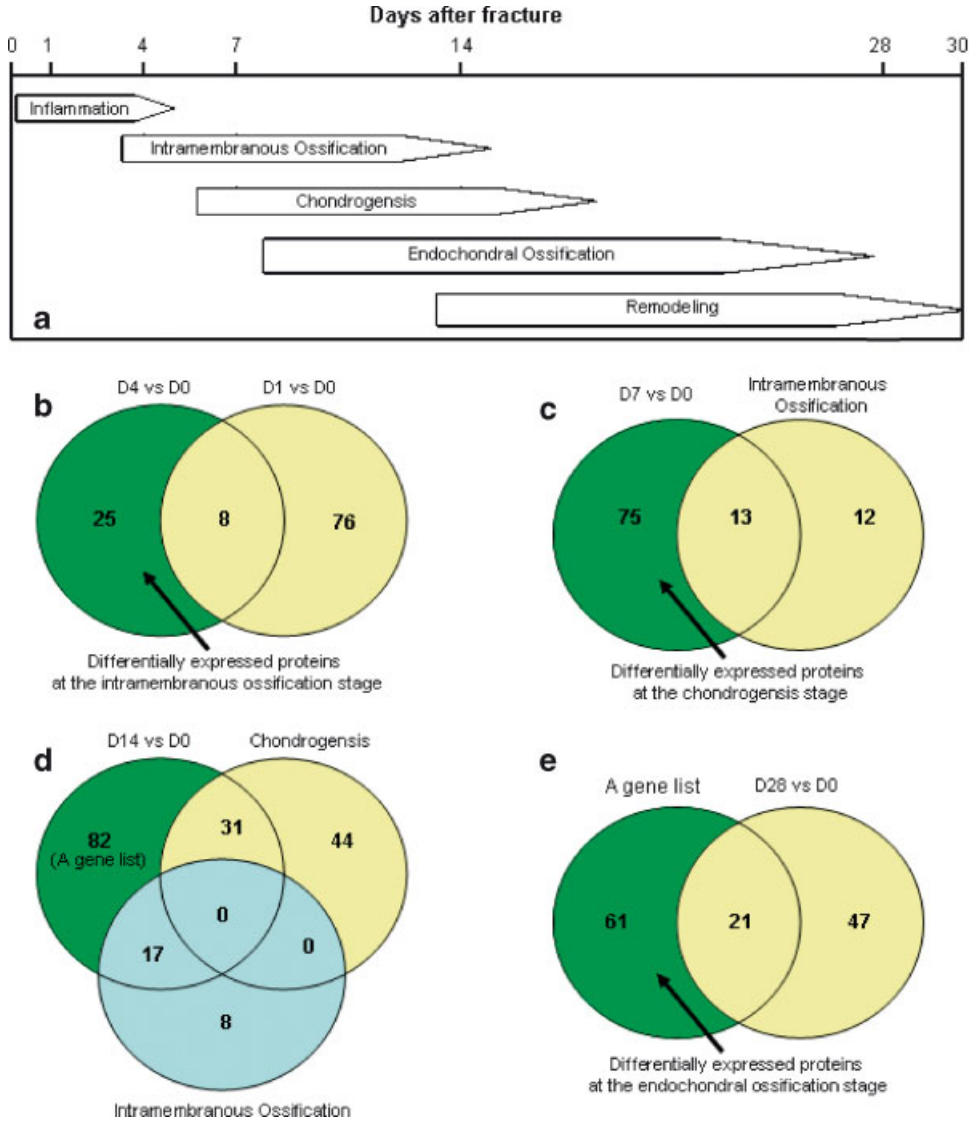

Fig. 1. Diagram showing the temporally interdependent cellular events during bone repair and the strategy for dissection of cellular event-specific proteins. **a**: Five interdependent cellular events during bone repair. Numbers on the top indicate days after fracture. Arrows indicate the approximate starting and end time of each event. The time line was drawn based on previous experimental data in this animal model [Jingushi et al., 1992] and descriptions in other models [Hadjiargyrou et al., 2002]. **b**: We adopted a minimum-number approach in the dissection of event-specific proteins (the minimum numbers of differentially expressed proteins in a specific cellular event at a particular time point). The differentially expressed proteins on Day 1 uniquely corresponded to inflammation event, while differentially expressed proteins on Day 4 corresponded to inflammation and intramembranous ossification. Thus, the minimum numbers of differentially expressed proteins at intramembranous ossification stage on Day 4 were equal to the differentially expressed proteins on Day 4 (Day 4 vs. Day 0) minus the commonly differentially expressed proteins between ''Day 1 versus Day 0'' and ''Day 4 versus Day 0''. **c**: Similarly, differentially expressed proteins on Day 7 corresponded to intramembranous ossification and chondrogenesis, the minimum numbers of differentially expressed proteins at chondrogenesis stage on Day 7 were equal to the differentially expressed proteins on Day 7 minus the commonly differentially expressed proteins between intramembranous ossification (as defined in b) and ''Day 7 versus Day 0''. **d**: The differentially expressed proteins on Day 14 corresponded to all stages except for inflammation stage. The 82 differentially expressed proteins (A gene list, which represents the differentially expressed proteins at endochondral ossification and/or remodeling) were first isolated by subtracting commonly differentially expressed proteins with intramembranous ossification (as defined in b) and/or chondrogenesis (as defined in c) from the comparison of ''Day 14 versus Day 0''. **e**: The minimum numbers of differentially expressed proteins at endochondral ossification stage on Day 14 were obtained by subtracting commonly differentially expressed proteins with the remodeling stage (Day 28 vs. Day 0) from the A gene list (as defined in d). Because false discovery rates for each time point comparison are all less than 3% (1.5% for D1 vs. D0, 2.1% for D4 vs. D0, 1.2% for D7 vs. D0, 1.5% for D14 vs. D0, and 2.7% for D28 vs. D0), the numbers shown in panels b, c, and e are unlikely due to random events. We further performed Fisher's exact test (based on the hypergeometric distribution) to see if the number of overlapped genes in panels b, c and e were significantly different from a random event. Results showed significance for panel c ($P < 0.001$) and panel e ($P < 0.01$),# but not for panel b ($P < 0.223$).

nodes, and the biological relationship between two nodes was represented as an edge (line). The intensity of the node color indicated the degree of up- (red) or downregulation (green). Nodes were displayed using various shapes that represent the functional class of the gene product. Edges were displayed with various labels that describe the nature of the relationship between the nodes (e.g., P for phosphorylation, T for transcription).

Networks were scored for the likelihood of finding the focus gene(s) in that given network. The higher the score, the lower the probability that you would find the focus gene(s) in a given network by chance. The *P*-scores were derived from *P*-values. Let's assume that there are n genes in the network and f of them are Focus Genes. The *P*-value is the probability of finding f or more Focus Genes in a set of n genes randomly selected from the Global Molecular Network. It was calculated using Fisher's exact test. Since interesting *P*-values are typically quite low (e.g., 10−8), it is visually easier to concentrate on the exponent. Therefore, the *P*-score is defined as: $P\text{-score} = -\log_{10}(P\text{-value})$.

Canonical pathway analysis. Canonical pathways analysis identified the pathways from the Ingenuity Pathways Analysis library of canonical pathways that were most significant to the data set. Genes from the data set that were associated with a canonical pathway in the Ingenuity Pathways Knowledge Base were considered for the analysis. The significance of the association between the data set and the canonical pathway was measured in two ways: (1) A ratio of the number of genes from the data set that map to the pathway divided by the total number of genes that map to the canonical pathway was displayed. (2) Fischer's exact test was used to calculate a *P*-value determining the probability that the association between the genes in the dataset and the canonical pathway is explained by chance alone.

Western Blotting

The same protein samples (10 μg) used for antibody arrays from Day 1 after fracture and intact controls were separated in 10% SDS–PAGE and transferred onto a nitrocellulose filter by means of a Mini Trans Blot apparatus (Bio-Rad) following the standard procedure. The filters were blocked at room temperature for 2 h with 1 X TBS/5% rat serum/0.1% TWEEN. They were then incubated at 4°C overnight with primary antibodies diluted in the blocking buffer. Monoclonal antibodies for GIT1, plakophilin 2a, dematin, and VHR were purchased from Pharmingen**.** The secondary antibody was AffiniPure Rat Anti-mouse IgG (H + L) from Jackson Immuno Research (1:400,000 dilution as suggested by the Pierce SuperSignal Western Femto detection system). The filters were washed and developed using SuperSignal Western Pico Detection system (Pierce Biotechnology). The optical densities (OD) were taken of X-ray images with the Kodak IDv3.6.0 software from Scientific Imaging Systems.

RESULTS

Dissection of Cellular-Event-Specific Proteins That Were Differentially Expressed During the Fracture Healing

Compared to non-fractured control, 84, 33, 88, 130, and 68 proteins were differentially expressed on Days 1, 4, 7, 14, 28, respectively. The FDR for these respective time points were 1.5, 2.1, 1.2, 1.5, and 2.7%. The complete lists for these five sets of data were published as supporting information at http://fgf.bsd.uchicago.edu/pickup/. Based on the time line of cellular events occurring during the progression of fracture healing and the numbers of differentially expressed proteins at each time point, we dissected the cellular event-specific changes using a minimum-number criterion (i.e., the minimum numbers of differentially expressed proteins in a specific cellular event at a given time point). Inflammation represents the first cellular event after fracture (Fig. 1a). The proteins differentially expressed on Day 1 coincide with this event. On Day 4, inflammation is close to the end and intramembranous ossification starts. Twenty-five differentially expressed proteins were specific to the intramembranous ossification stage on Day 4, which were derived by subtracting proteins that overlapped between Day 1 versus Day 0 and Day 4 versus Day 0 (the overlapped proteins were either inflammation-related proteins or proteins functioning at both cellular events, Fig. 1b). Using a similar strategy (see Fig. 1 legend for detailed description of dissection of cellular-event-specific proteins at other time point), 75 differentially expressed proteins were identified to be specific to chondrogenesis on Day 7 (Fig. 1c) and 61 specific to endochondral

ossification on Day 14 (Fig. 1e). Proteins differentially expressed on Day 28 primarily correspond to remodeling events. The complete lists for the cellular-event-specific proteins at a given time point were published as supporting information at http://fgf.bsd.uchicago.edu/pickup/.

Characterization of Differentially Expressed Proteins at Each of the Key Cellular Events During Fracture Healing

Characterization of the differentially expressed proteins at each cellular event followed a three-step strategy. First, we constructed genetic networks to reveal physical or functional relationships among the differentially expressed proteins. Second, we performed a high level analysis to identify functional groups associated with those proteins. Finally, we carried out pathway analyses to identify statistically enriched pathways that coincided with a specific cellular event.

Inflammation. To functionally characterize the list of the differentially expressed proteins on Day 1 (inflammation stage), we mapped those proteins to genetic networks as defined by the Ingenuity Knowledge-Based database. Seventy-six of 84 differentially expressed proteins mapped to five highly significant networks (Score $\geq$10, Table I). These networks were associated with cell cycle, cellular assembly and organization, cell-to-cell signaling and interaction, protein synthesis, nucleic acid metabolism, lipid metabolism, and molecular transport. High level analysis identified that 28 of these 76 proteins (37%) were associated with cell cycle (20 out of 28 were upregulated), which represents the most significant functional group ($P = 1.68\text{E}^{-8}$–3.60E^{-2}) either compared to all other stages within the group or compared to all other functional groups at the inflammation stage. All mitogenesis and S phase-related proteins were upregulated (EGFR, IGFBP3, PIK3R1, PRKCA, CCND2, HMOX1, E2F2, and TFDP1), while meiosis-related proteins were downregulated (MLH1 and PPP1R2). Pathway analysis identified six significant signaling pathways that were potentially functioning during the inflammation stage (Fig. 2 top panel and Table II). Of those, IGF-1 and PDGF signaling are well known pathways involved in bone repair.

Intramembranous ossification. Twenty-five proteins were uniquely differentially expressed at the intramembranous ossification-stage (Day 4), which represent the smallest group of differentially expressed proteins compared to other cellular events. Sixteen of 23 mapped proteins fell into a single interacting network. This network is significantly associated with cell death, immune response, and cell signaling. Twenty-four proteins on the network were classified as cell death related ($P = 4.64\text{E}^{-14}$–5.23E^{-3}), representing 69% of the networked proteins. IL-6 (twofold increase) is centered in the network, which is known to be a key regulator for the above mentioned three functional groups. Consistent with the network functional analysis, high level analysis on 23 differentially expressed proteins revealed that cell death was the most abundant functional group (12 proteins accounting for 52% of the mapped proteins), while cell growth and proliferation was the most significant functional category ($P = 1.32\text{E}^{-5}$–4.72E^{-2}). Of 12 cell death-related proteins, 9 were downregulated (BIRC6, CD28, DAP3, DOK2, FUBP1, GRAP2, MGMT, SLC9A1, and VIL2).

Chondrogenesis. Chondrogenesis represents the most active molecular stage (Day 7). Seventy-five proteins were differentially expressed and 62 mapped to three genetic networks (Table I), which merged into a giant network bridged by CHUK, NR3C1, MAP3K1, and CDK7 (Fig. 3). Sixty-two global analysis genes were significantly associated with cell death, gene expression, cellular growth and proliferation, cell morphology, cellular assembly and organization, and nerve system development and function (Fig. 4 top panels). Cell death was identified as the most significant ($P = 2.21\text{E}^{-10}$–7.52E^{-3}) and abundant functional category. Thirty-five proteins were cell death-related accounting for 57% of the mapped global analysis proteins (Table III). Five of the six significant functional groups fell into the molecular and cellular function category (only nervous system development and function belongs to the physiological system development and function category). Twelve molecular pathways were potentially active during chondrogensis, including PDGF, VEGF, PPAR, and B cell receptor pathways (Fig. 2). Of 12 enriched pathways, the P13K/AKT (signaling cell survival) represents the most significant pathways ($P = 1.27\text{E}^{-4}$).

Endochondral ossification. Coinciding with endochondral ossification (Day 14), 61 proteins were uniquely, differentially expressed

TABLE I. Genetic Networks Identified at Each Cellular Event During the Bone Repair

Analysis	Network ID	Genes in network*	P-score	Focus genes	Top categories
Inflammation	1	APOC3, ARNT, **CCL2**↑, **COL7A1**↑, **CTBP2**↑, DDB2, EP300, **FEN1**↑, **FKBP1A**↑, GATA5, GATA6, **IGFBP3**↑, **MAPK13**↑, MDM4, **NONO**↑, **PCMT1**↑, PIAS1, PPP1CA, **PPP1R2**↓, PPP1R9B, PRKDC, **PRKR**↑, SFPQ, **SMAD4**↑, SP1, STK11, **STMN1**↑, **TAF6**↑, **TANK**↑, TOP1, TP53, **UBE2I**↓, **WRN**↓, **XRCC4**↑, YY1	26	18	Cell death, gene expression cell cycle
	2	**ADAM9**↑, APP, BRD2, **CALD1**↓, **CCND2**↑, CCNE, **CDC2**↓, **CDC25C**↑, CDK2, CDT1, CKS1B, CNOT7, **CUL2**↓, **CYCS**↑, **E2F2**↑, E2F5, **EDNRA**↑, **HMOX1**↑, HTATIP, **ITCH**↑, **LZTS1**↓, MAP4, MED8, MYC, NPDC1, P44S10, PRDX1, **PSMC5**↑, RBX1, SE20-4, SFN, SMAD3, **TEBP**↑, **TFDP1**↑, UBE2A	20	15	Cell cycle, cellular assembly and organization, DNA replication/ recombination/ repair
	3	ABCB1, **ANXA11**↑, AREG, **BLNK**↓, CBLB, CEBPB, CTNNB1, DCN, **EGFR**↑, **IL5**↑, JUP, KIF23, MUC1, NPHS1, NRG1, **PIK3CA**↑, PIK3CB, PIK3CD, PIK3CG, **PIK3R1**↑, PIK3R2, PIK3R3, **PKP2**↑, **PLEK**↑, PRKAR1A, **PRKAR2B**↑, **PTPRF**↓, SH3KBP1, **SMARCA2**↑, **SNX1**↑, SNX2, SNX6, **TRIM28**↑, VAV3, **WT1**↑	18	14	Cellular growth and proliferation, hematological system development and function, cell death
	4	BENE, **BET1L**↑, **BIRC4**↑, **BMX**↑, CACNA1A, CASP3, CAV1, **CAV2**↑, **CCNC**↑, **CNTN1**↓, **EIF4G1**↑, EIF4G3, FLOT1, **FLOT2**↓, FYN, GNAQ, GPAA1, **GSN**↓, ITPR1, MKNK2, **MLH1**↓, **NCOR2**↑, PLCB1, PPARBP, PPARG, PRNP, PTK2, **SEC8L1**↑, SNAP25, **STIM1**↓, STX16, **SYT1**↑, TNFRSF1B, VTI1A, VTI1B	18	14	Cellular development, connective tissue development and function, organ morphology
	5	AKT1, CBL, **DLG1**↑, **DUSP3**↑, **EIF5**↓, FMR1, FYN, **GIT1**↑, GNAI2, GNAS, **GNB1**↓, **GNB2L1**↓, GNG2, GRK4, HABP4, ITGB1, LCK, MLPH, MPZ, MYO5A, **MYO5B**↑, MYO5C, MYRIP, **PRKCA**↑, PRKCB1, PRKCD, **PRKCI**↑, PTPN11, RAB27A, RAB3A, **RPH3A**↑, SRC, STAU, **TMPO**↑, **ZAP70**↓,	15	12	Cell-to-cell signaling and interaction, cellular assembly and organization, cell signaling
Intramembranous ossification	1	**CAV1**↑, **CD28**↓, **CDC27**↑, **DAP3**↓, **DOK2**↓, **EIF4E**↑, FMR1, **FUBP1**↓, GAB2, GAB3, **GRAP2**↓, GRB2, HMGB1, **IL6**↑, LAX, LCK, MAPK3, MYC, NR3C1, NSEP1, PURA, **RAB4A**↑, **RAG1**↑, RELA, **SLC9A1**↓, SMAD3, SOS2, **SRPK1**↑, TBP, **TEAD1**↓, TNFRSF10A, TNFSF5, TP53, **VIL2**↓, **WASF1**↓,	33	16	Cell death, hematological disease, immunological disease
Chondragensis	1	BBC3, **BCL2**↓, CASP8AP2, **CD3Z**↑, **CDK4**↓, **CDK7**↓, CHUK, **E2F1**↑, **FADD**↓, **HSPCA**↑, **ITGB1**↓, **KSR**↑, **L1CAM**↑, MAP2K2, MAP3K1, MAP3K7, **MAPK1**↓, **MDM2**↑, MDM4, **MSH2**↓, **NCOA3**↓, **NFATC2**↑, P53AIP1, PAWR, PMAIP1, POU4F2, SERTAD1, SLC3A2, **SMAD4**↓, **SMARCA2**↓, TNFSF9, TP53BP2, **TP73**↑, **TRAF2**↓, **WT1**↑	33	20	Cell death, gene expression, cancer
	2	**ARHGDIA**↑, BRF1, **CDK7**↓, **CHD3**↓, CSNK1D, **CTBP2**↑, CYBA, DUSP10, **DUSP4**↓, **ILK**↓, LIG4, **LSP1**↑, MAP3K1, MAPK8, **MAPT**↓, **NCF1**↓, NCF4, **NONO**↓, NR3C1, POLM, **PRKCB1***↓, **PTEN**↑, RAC1, RAC2, RB1, **SNCA**↓, **TERF2**↑, TERF2IP, TOP1, TOP2A, TP53, UBE2I, WWOX, **XRCC4**↑, XRCC5	22	15	DNA replication, recombination, and repair, free radical scavenging
	3	ACP1, **AMPH**↑, APPL, CASP3, CDC2, CHC1, CHUK, **CTBP1**↑, CTNNB1, CTNND1, **DCC**↑, **EDNRA**↑, FKBP4, **FKBP5**↓, HDAC1, HDAC9, HTATIP, **IL3**↓, **MAP4**↑, **MATK**↓, MYC, NR3C1, **PDGFRB**↑, PECAM1, **PIK3CA**↑, PIK3CB, PIK3CD, PIK3CG, **PKN2**↓, **PKP2**↓, PLA2G4A, **PLEK**↑, **PTPN6**↑, RUNX1, SRC	20	14	Cellular growth and proliferation, cell death, cellular development

(*Continued*)

TABLE I. (*Continued*)

Analysis	Network ID	Genes in network*	P-score	Focus genes	Top categories
Endochondral ossification	1	**ANXA2**↑, **CDKN1A**↑, **CREBBP**↑, **CTSL**↓, **CYCS**↑, DDX5, **DHFR**↓, ENO1, FDX1, **GTF2B**↑, **HIF1A**↓, HMGN2, **HSPD1**↑, **IGFBP3**↓, LDHA, MAZ, **MYC**↑, **NFATC2**↓, **PEX19**↓, PGK1, PIM1, PRKACB, **PRKAR1B**↑, RPL19, RPL22, RPL7, RPS13, RPS18, RPS19, RPS4X, **STAT2**↑, **THRSP**↓, TLE4, **TNF**↑, TYMS	27	17	Cancer, cellular development, hair and skin development and function
	2	**ADPRT**↓, BCL3, **BIK**↑, **CASP4**↑, **CCL2**↓, CDC42, CEBPB, CHEK2, **CSF2**↑, CSF2RA, **DHFR**↓, ELL, EP300, FOS, FRK, HAS2, **IL5**↓, MAF, MCM5, **MCM6**↑, ODC1, **PLK3**↑, POLB, PTGS2, RB1, **SMN1**↓, STX1A, **STXBP5**↓, **SYT1**↓, TEP1, **TNF**↑, TP53, **TRIM28**↓, WRN, **XPA**↑	23	15	Cell death, connective tissue disorders, cell cycle
	3	**ADAM9**↑, ALK, APP, **CCNDBP1**↓, CDH2, **CDH5**↑, CLDN1, CTTN, EGFR, F11R, FGFR4, FRS2, **GAP43**↓, GJA1, GNAQ, GRAP2, **HAX1**↓, HCLS1, KIT, **MLLT4**↑, **MPDZ**↑, NCAM1, NTRK2, PLCB1, PLCG1, PVR, PVRL2, **SEC8L1**↓, **SHC3**↑, **SNAP91**↓, **SNX1**↓, SNX6, SRC, TJP1, TRPC1	15	11	Cell morphology, cellular assembly and organization, nervous system development and function
	4	**BCAR1**↓, BRAF, CBLB, CD3E, CD79A, CDC37, **CRK**↑, CRKL, **DLG1**↓, DOCK1, **DUSP3**↓, GAB2, IRS4, JAK3, LAT, LAX, **LCK**↑, LCP2, MAP3K3, MAP4K1, **NFKBIA**↓, PRKCE, PRKCM, PTPN1, PTPRC, PTPRCAP, PXN, RAPGEF1, **RIN1**↑, SIT, YWHAB, YWHAE, YWHAH, YWHAZ, **ZAP70**↑	10	8	Cell-to-cell signaling and interaction, cellular function and maintenance, hematological system development and function
Remodeling	1	APAF1, AXIN2, BCL2, **BCLAF1**↓, **BIRC4**↓, CASP10, **CASP14**↑, CASP3, CASP4, CASP6, CASP8, CTNNB1, **DCC**↑, DVL1, EIF2S1, FLJ14639, **GSK3B**↑, **ILK**↓, ILKAP, JUP, LTBR, **MAPRE1**↑, PAWR, PKN2↓, PKP2↓, PRKCQ↓, PRKR↓, **SRPK1**↑, **STRAP**↑, TANK, TGFBR1, TNFRSF10A, **TP53BP2**↑, TRAF1, **TRAF4**↓,	22	15	Cell death, post-translational modification, renal and urological disease
	2	AKAP1, **AKAP9**↓, **ARHGAP5**↑, CHX10, **DIAPH1**↑, ETV3, F3, **FLNA**↑, FOS, **HSPA1A**↓, ICAM1, **KCNMA1**↓, MAP2, **MSN**↓, MYC, MYCBP, **NCOR2**↓, PDE4D, PIP5K1B, PRKACA, PRKACB, **PRKAR2B**↑, PRRX1, **PSMC5**↓, **PTEN**↑, RB1, RBBP9, **RBL2**↑, RHOA, **ROCK2**↓, SKIIP, SPN, **TMPO**↓, USP4, UXT	20	14	Lipid metabolism, dermatological diseases and conditions, organismal injury and abnormalities
	3	ACP1, ANXA2, CAV1, CD47, CD53, CEACAM6, **DNM2**↑, EDG1, **EIF4E**↑, **F11R**↑, FAP, **GIT1**↓, GJA1, GJA3, GNB2L1, **GRB14**↓, ITGA1, **ITGA3**↑, **ITGB1**↓, LAMA2, LAMC2, **LSP1**↑, MCP, **PDGFRB**↑, PIK4CA, PRKCB1, **PRKR**↓, PTPRA, RELN, **SNCA**↓, SRC, **TJP1**↑, TM4SF3, TM4SF7, **TUBB**↑	18	13	Cellular movement, cell-to-cell signaling and interaction, hair and skin development and function
	4	**CCNC**↑, **CDH3**↑, CGI-125, CREBBP, **CSK**↓, **CYBB**↓, **DAP3**↓, EPHA2, GAB3, **GRAP2**↓, GRB2, **IL3**↓, IRS3, **KHDRBS1**↓, KHDRBS2, LAX, MGMT, NPHS1, NR3C1, **PIK3CA**↑, PIK3CB, PIK3CD, **PIK3R1**↑, PIK3R3, PPARBP, PTPN22, RUNX1, SLC2A4, SMAD4, SOS2, TOM1L1, **TP73**↑, **UBE2I**↑, VAV3, **WASF1**↓	18	13	Cancer, cellular growth and proliferation, respiratory disease

A score of >10 was considered as significant network.
*Bold proteins were those differentially expressed in relative to non-fractured control. Other proteins were either not on the array or not significantly changed. Up/down arrows stand for up/down regulation.

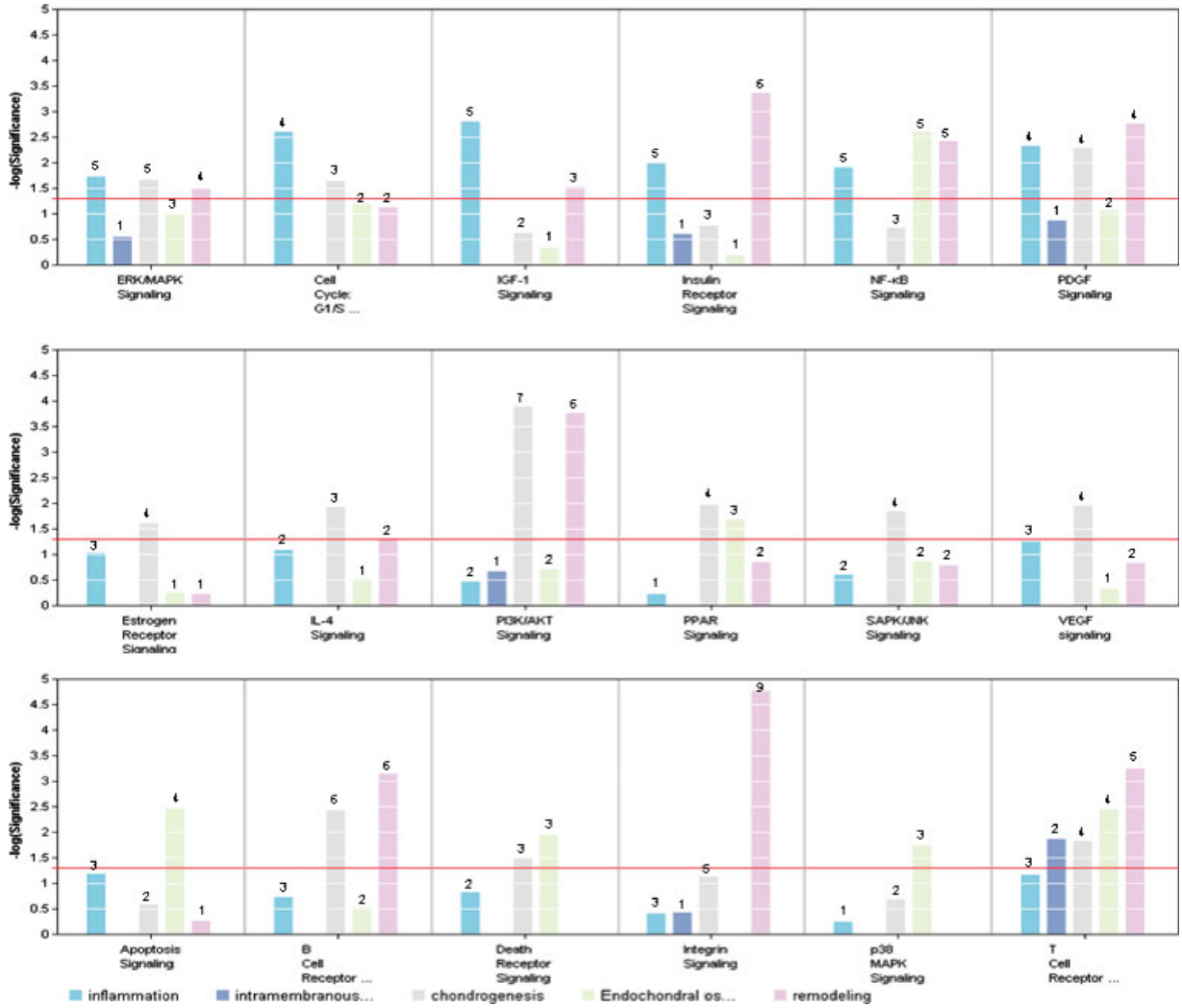

Fig. 2. Significantly enriched pathways at five cellular events of bone repair. Y axis is log-#transformed significance. $P = 0.05$ is equivalent to y value of 1.3 (red line). The number on the **top** of bar represents differentially expressed proteins falling into that molecular pathway. The bars from **left** to **right** for each pathway represent inflammation, intramembranous ossification, chondrogenesis, endochondral ossification, and remodeling, respectively.

and 56 mapped to four genetic networks. This group of proteins is significantly associated with development and function of cardiovascular, hematological, immune and lymphatic systems, organismal and cellular development, and DNA replication/recombination/ repair (Fig. 4 bottom panels). Different from the chondrogenesis-related proteins, four out of the six functional groups fell into physiological system development and function category, while only cellular development and DNA replication/recombination/repair belong to the molecular and cellular function category (as defined by the Ingenuity Pathway Analysis). Pathway analysis suggests that at least six pathways were potentially active at the endochondral ossification stage (Fig. 2). Of the six, PPAR, death receptor, and T-cell receptor signaling were also identified at the chondrogenesis stage, while apoptosis and p38/MAPK signaling were uniquely significant at this stage.

Remodeling. Sixty-eight proteins were differentially expressed at this stage (Day 28). Carbohydrate metabolism was the most significantly enriched functional group compared to other cellular events within this group and across all other groups. The differentially expressed proteins involved in the carbohydrate

TABLE II. Summary of Significantly Enriched Pathways and Related Proteins

Cellular event	Pathway	*P*-value	Genes
Inflammation	IGF-1 Signaling	1.52E-3	PIK3CA↑, IGFBP3↑, PIK3R1↑, PRKAR2B↑, PRKCI↑
	Cell cycle: G1/S checkpoint regulation	2.43E-3	E2F2↑, CCND2↑, SMAD4↑, TFDP1↑
	PDGF signaling	4.50E-3	PIK3CA↑, PRKCA↑, PIK3R1↑, PRKR↑
	Insulin receptor signaling	1.01E-2	PIK3CA↑, PIK3R1↑, PTPRF↓, PRKAR2B↑, PRKCI↑
	NF-κB signaling	1.19E-2	PIK3CA↑, EGFR↑, ZAP70↓, PIK3R1↑, PRKR↑
	ERK/MAPK signaling	1.83E-2	PIK3CA↑, PRKCA↑, PIK3R1↑, PRKAR2B↑, PRKCI↑
Intramembranous ossification	T-cell receptor signaling	1.33E-2	CD28↓, GRAP2↓
Chondrogensis	PI3K/AKT signaling	1.27E-4	PIK3CA↑, MDM2↑, MAPK1↓, ILK↓, HSPCA↑, PTEN↑, BCL2↓
	B cell receptor signaling	3.57E-3	PIK3CA↑, NFATC2↑, MAPK1↓, PTPN6↑, PRKCB1*↓, PTEN↑
	PDGF signaling	5.08E-3	PIK3CA↑, PDGFRB↑, MAPK1↓, PRKCB1*↓
	PPAR signaling	1.06E-2	TRAF2↑, PDGFRB↑, MAPK1↓, HSPCA↑
	VEGF signaling	1.12E-2	PIK3CA↑, MAPK1↓, PRKCB1*↓, BCL2↓
	IL-4 signaling	1.16E-2	PIK3CA↑, NFATC2↑, PTPN6↑
	SAPK/JNK signaling	1.38E-2	TRAF2↑, PIK3CA↑, FADD↓, DUSP4↓
	T-cell receptor signaling	1.45E-2	PIK3CA↑, CD3Z↑, NFATC2↑, MAPK1↓
	ERK/MAPK signaling	2.09E-2	PIK3CA↑, DUSP4↓, MAPK1↓, KSR↑, PRKCB1*↓
	Cell cycle: G1/S checkpoint regulation	2.16E-2	CDK4↓, E2F1↑, SMAD4↓
	Estrogens receptor signaling	2.36E-2	CTBP2↑, CTBP1↑, NCOA3↓, MAPK1↓
	Death receptor signaling	3.18E-2	TRAF2↑, FADD↓, BCL2↓
Endochondral ossification	NF-κB signaling	2.38E-3	NFKBIA↓, CREBBP↑, ZAP70↑, LCK↑, TNF↑
	Apoptosis signaling	3.30E-3	NFKBIA↓, CYCS↑, TNF↑, ADPRT↓
	T-cell receptor signaling	3.48E-3	NFKBIA↓, ZAP70↑, LCK↑, NFATC2↓
	Death receptor signaling	1.10E-2	NFKBIA↓, CYCS↑, TNF↓
	p38 MAPK signaling	1.72E-2	EEF2K↑, TNF↑, MYC↑
	PPAR signaling	2.04E-2	NFKBIA↓, CREBBP↑, TNF↑
Remodeling	Integrin signaling	1.69E-5	ITGB1↓, ARHGAP5↑, PIK3CA↑, ITGA3↑, GIT1↓, GSK3B↑, PIK3R1↑, ILK↓, PTEN↑
	PI3K/AKT signaling	1.70E-4	PIK3CA↑, GSK3B↑, PIK3R1↑, ILK↓, EIF4E↑, PTEN↑
	Insulin receptor signaling	4.09E-4	PIK3CA↑, GSK3B↑, PIK3R1↑, PRKAR2B↑, EIF4E↑, PTEN↑
	T-cell receptor signaling	5.56E-4	CSK↓, PRKCQ↓, PIK3CA↑, PIK3R1↑, GRAP2↓
	B cell receptor signaling	6.80E-4	CSK↓, PRKCQ↓, PIK3CA↑, GSK3B↑, PIK3R1↑, PTEN↑
	PDGF signaling	1.64E-3	PIK3CA↑, PDGFRB↑, PIK3R1↑, PRKR↓
	NF-κB signaling	3.64E-3	PRKCQ↓, PIK3CA↑, GSK3B↑, PIK3R1↑, PRKR↓
	IGF-1 signaling	2.83E-2	PIK3CA↑, PIK3R1↑, PRKAR2B↑
	ERK/MAPK signaling	2.96E-2	PIK3CA↑, PIK3R1↑, PRKAR2B↑, EIF4E↑
	IL-4 signaling	4.87E-2	PIK3CA↑, PIK3R1↑

metabolism include ITGB1, PDGFRB, PIK3CA, PIK3R1, PTEN, and UBE-2I (all were upregulated except for ITGB1). Ten molecular pathways potentially participate in the remodeling phase, of which integrin signaling is particularly interesting (Fig. 2). Nine differentially expressed proteins fell into the integrin-signaling pathway (six of those were upregulated), representing the most significantly enriched pathway across all cellular events of all pathways in terms of *P*-value and the number of proteins.

Confirmation of Protein Array Data

Verification of protein array-based differential protein expression was performed on four representative proteins by using Western blot analysis. These four proteins were upregulated one day after fracture based on protein array results. Figure 6 showed the same direction of differential expression of those proteins by Western blot analysis.

DISCUSSION

Despite the advances in understanding of the molecular mechanisms of fracture repair, specific molecular pathways contributing to a given cellular event have remained elusive. Accordingly, there is considerable interest in elucidating interactive networks and molecular pathways that regulate bone fracture repair. We and others have identified many signaling molecules potentially associated with bone repair using transcriptional profiling [Hadjiargyrou et al., 2002; Hatano et al., 2004; Nakazawa et al., 2004; Li et al., 2005]. In this study, we examined protein profiles over the 28-day period of bone repair, which provide more directly relevant data to events occurring post-fracture. We first dissected out cellular-event-specific changes and then revealed key interacting networks and molecular pathways that are associated with a given cellular event.

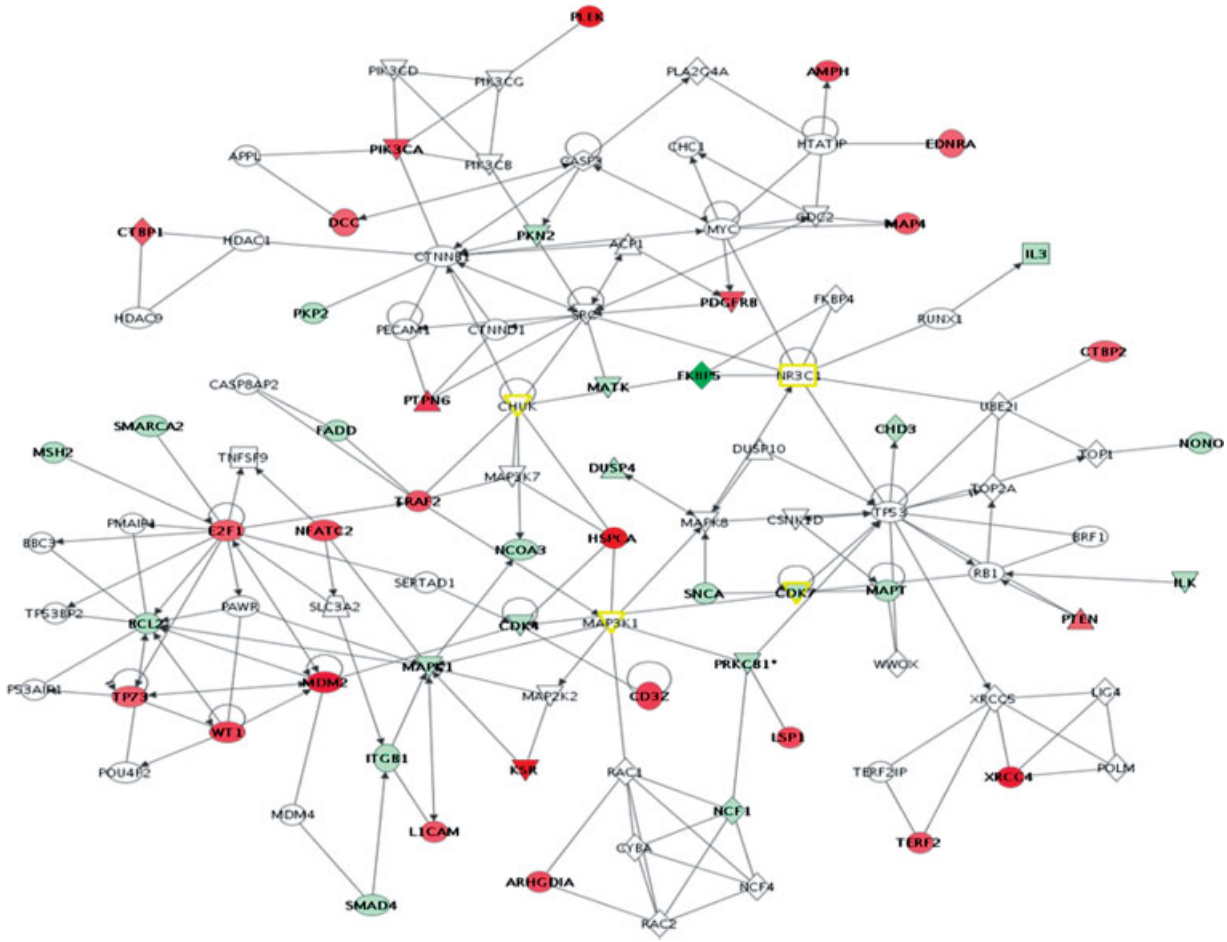

Fig. 3. A merged genetic network showing physical or functional interactions among proteins at the phase of chondrogenesis (Day 7). Red and green-color represent up- and downregulated proteins. Yellow-colored proteins indicate merging points of the original three networks.

The first event after fracture is bleeding from the damaged bone end. The accumulated blood forms a hematoma at the fracture site and then initiates an inflammatory response to prepare for bone repair. On Day 1, the multiple inflammatory cell types exist in the hematoma mainly including monocytes, macrophages, and neutrophils. These cells provide and respond to cytokines creating the first environment critical for fracture healing [Rosen and Thies, 1995]. Functional analysis showed that the molecular sense of preparation for fracture healing includes two aspects. One is the production of essential materials leading to increased expression of cell cycle-related proteins. The regulation of the cell cycle seems to be a central theme during this phase (accounting for 37% of the differentially expressed proteins, of which 72% were upregulated). Increased expression of cell cycle-related proteins provides a molecular foundation for the previous observation that cell division reached a maximum in some 24 h after fracture [McKibbin, 1978]. In this regard, upregulation of EGFR (2.7-fold) is particularly significant. This growth factor plays a critical role in many stages of the cell cycle, including G1-, G2-, and S-phases and regulates multiple proteins important for cell growth (Fig. 5). It is reasonable to assume that therapeutic approaches to temporally promote expression of EGFR might be beneficial for the early stage of bone repair. The second aspect of this molecular preparation is attributable to cell-to-cell signaling, which is essential to initiate bone repair. Of those, IGF-1, NF-Kb, and PDGF signaling are well known to be involved in bone repair while

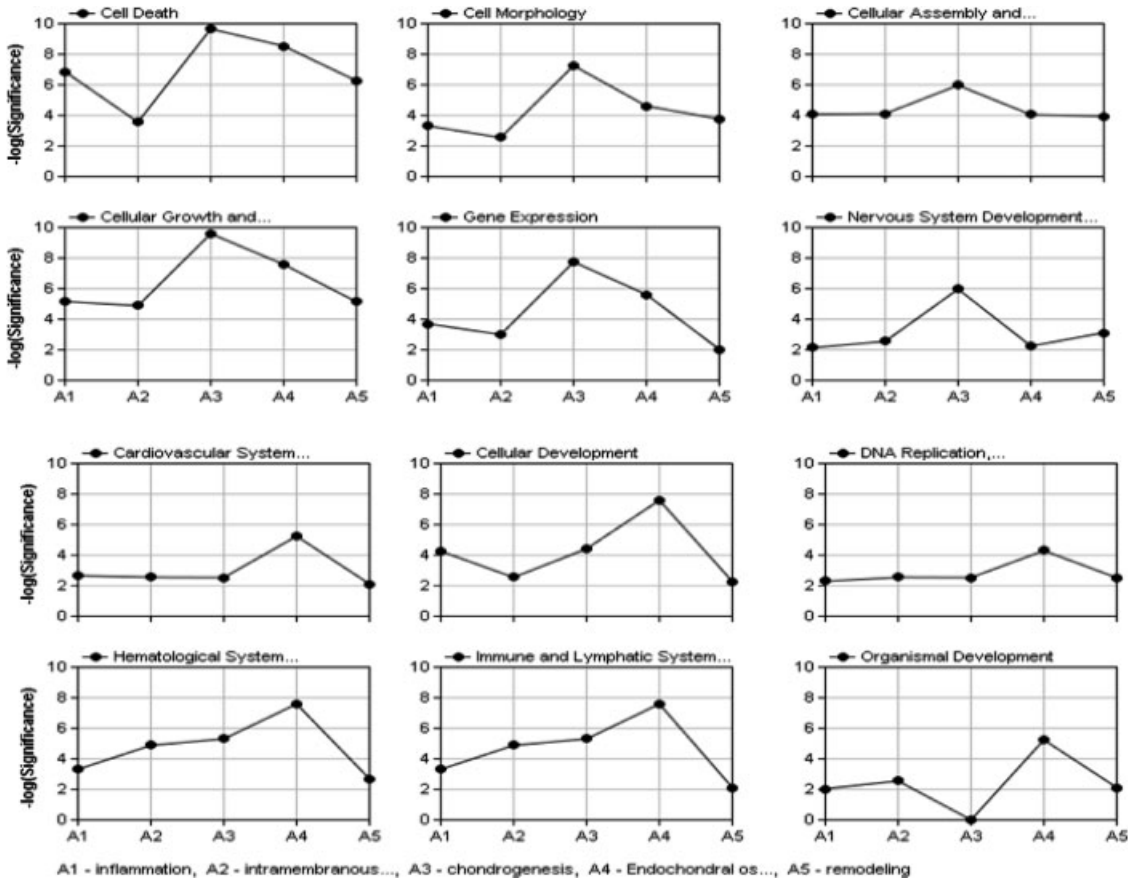

Fig. 4. Comparison of significant enrichments of high level function among five cellular events. The y axis is log-transformed significance ($P = 0.001$ is equivalent to y value of 3). A1-inflammation (Day 1), A2-intramembranous ossification (Day 4), A3-chondrogenesis (Day 7), A4-endochondral ossification (Day 14), A5-remodeling (Day 28).

ERK/MAPK and insulin-receptor signaling remain to be fully defined during bone repair.

On Day 4, soft callus forms around the fractured sites and with it comes a population of undifferentiated mesenchymal cells that invades soft callus. The healing site is filled with a small amount of well-vascularized-connective tissue that has been converted from hematoma by the infiltration and proliferation of endothelial cells and fibroblasts. Macrophages continue to remove debris, while number of neutrophils decline. In the meantime, the red blood cells and platelets initiate angiogenesis [Hulth, 1989; Jingushi et al., 1992]. Osteoblast progenitor cells in the inner layer of periosteum differentiate and synthesize non-permanent bone matrix, a process called intramembranous ossification. Molecularly, intramembranous ossification is a relatively quiet stage. Only 25 proteins were differentially expressed in relative to the non-fractured control. Interestingly, over 50% of mapped proteins were cell death-related, most of which were downregulated. It seems that the central molecular activity shifts from regulating the cell growth at the inflammation stage to regulating cell death at the intramembranous ossification phase.

On Day 7, hematoma and fibrinous clot are restricted to a much smaller area at the fracture ends and are encircled by macrophages. Bulging fibrovascular tissue forms a soft callus that bridges the fracture ends and connects to the periosteal bony proliferation on the viable segments of the cortical bone. Chondroblasts, osteoblasts, and fibroblasts are abundant, while scattered neutrophils and lymphocytes are seen randomly distributed in the soft callus. Osteoclasts have started to resorb the newly formed trabecular bone [Jingushi et al., 1992]. This

TABLE III. Cell Death-Related Proteins at Chondrogenesis

Protein name	Locus link	Fold change	Description	Family	Location
ARG1	383	1.939	Arginase, liver	Enzyme	Cytoplasm
BCL2	596	−2.277	B-cell CLL/lymphoma 2		Cytoplasm
CASP14	23,581	1.906	Caspase 14, apoptosis-related cysteine protease	Peptidase	Cytoplasm
CD3Z	919	1.897	CD3Z antigen, zeta polypeptide (TiT3 complex)	Transmembrane receptor	Plasma membrane
CDK4	1,019	−2.165	Cyclin-dependent kinase 4	Kinase	Nucleus
DCC	1,630	1.502	Deleted in colorectal carcinoma	Transmembrane receptor	Plasma membrane
E2F1	1,869	1.585	E2F transcription factor 1	Transcription regulator	Nucleus
FADD	8,772	−1.861	Fas (TNFRSF6)-associated via death domain		Cytoplasm
IL3	3,562	−1.935	Interleukin 3 (colony-stimulating factor, multiple)	Cytokine	Extracellular Space
IL12A	3,592	−2.248	Interleukin 12A (natural killer cell stimulatory factor 1	Cytokine	Extracellular Space
ILK	3,611	−2.918	Integrin-linked kinase	Kinase	Plasma membrane
ITGB1	3,688	−3.628	Integrin, beta 1	Transmembrane receptor	Plasma membrane
KSR	8,844	3.029	Kinase suppressor of ras	Kinase	Cytoplasm
L1CAM	3,897	1.69	L1 cell adhesion molecule		Plasma membrane
LSP1	4,046	1.808	Lymphocyte-specific protein 1		Cytoplasm
MAP4	4,134	1.677	Microtubule-associated protein 4		Cytoplasm
MAPK1	5,594	−2.938	Mitogen-activated protein kinase 1	Kinase	Cytoplasm
MAPT	4,137	−2.972	Microtubule-associated protein tau		Cytoplasm
MDM2	4,193	2.292	Mdm2, p53 binding protein	Transcription regulator	Nucleus
MSH2	4,436	−2.644	mutS homolog 2, colon cancer, nonpolyposis type 1 (E. coli)		Nucleus
NCOA3	8,202	−1.977	Nuclear receptor coactivator 3	Transcription regulator	Nucleus
NFATC2	4,773	1.804	Nuclear factor of activated T-cells	Transcription regulator	Nucleus
PDGFRB	5,159	1.751	Platelet-derived growth factor receptor, beta polypeptide	Kinase	Plasma membrane
PIK3CA	5,290	1.831	Phosphoinositide-3-kinase, catalytic, alpha polypeptide	Kinase	Cytoplasm
PKN2	5,586	−2.629	Protein kinase N2	Kinase	Cytoplasm
PRKCB1	5,579	−1.877	Protein kinase C, beta 1	Kinase	Cytoplasm
PTEN	5,728	1.536	Phosphatase and tensin homolog	Phosphatase	Cytoplasm
PTPN6	5,777	1.95	Protein tyrosine phosphatase, non-receptor type 6	Phosphatase	Cytoplasm
SMAD4	4,089	−1.754	SMAD, mothers against DPP homolog 4 (Drosophila)	Transcription regulator	Nucleus
SMARCA2	6,595	−2.733	SWI/SNF related, actin dependent regulator of chromatin	Transcription regulator	Nucleus
SNCA	6,622	−1.753	Synuclein, alpha (non A4 component of amyloid precursor)		Cytoplasm
TP73	7,161	1.533	Tumor protein p73	Transcription regulator	Nucleus
TRAF2	7,186	1.698	TNF receptor-associated factor 2		Cytoplasm
WT1	7,490	1.89	Wilms tumor 1	Transcription regulator	Nucleus
XRCC4	7,518	2.418	X-ray repair complementing defective repair in Chinese hamster cells 4		Nucleus

study showed that chondrogenesis on Day 7 represents the molecularly most active stage among the five cellular events. This high level of activity correlates well with the biological events at this repair stage, characterized by dramatic physical changes in cell type, number, size, and shape as well as constituents of the extracellular matrix (ECM). The majority of the differentially expressed proteins fall into one giant genetic network indicating the complex, interdependent nature of the genes' function (Fig. 3). This close correlation among the differentially expressed proteins is biologically expected because these proteins at this stage are presumably working together toward the same end: forming the new bone. Many genes on this network belong to signaling pathways of the B cell receptor (15), SAPK/JUK (14), ERK/MAPK (13), PI3K/AKT (13), PDGF (12), T-cell receptor (10), PPAR (7), estrogen receptor (7),

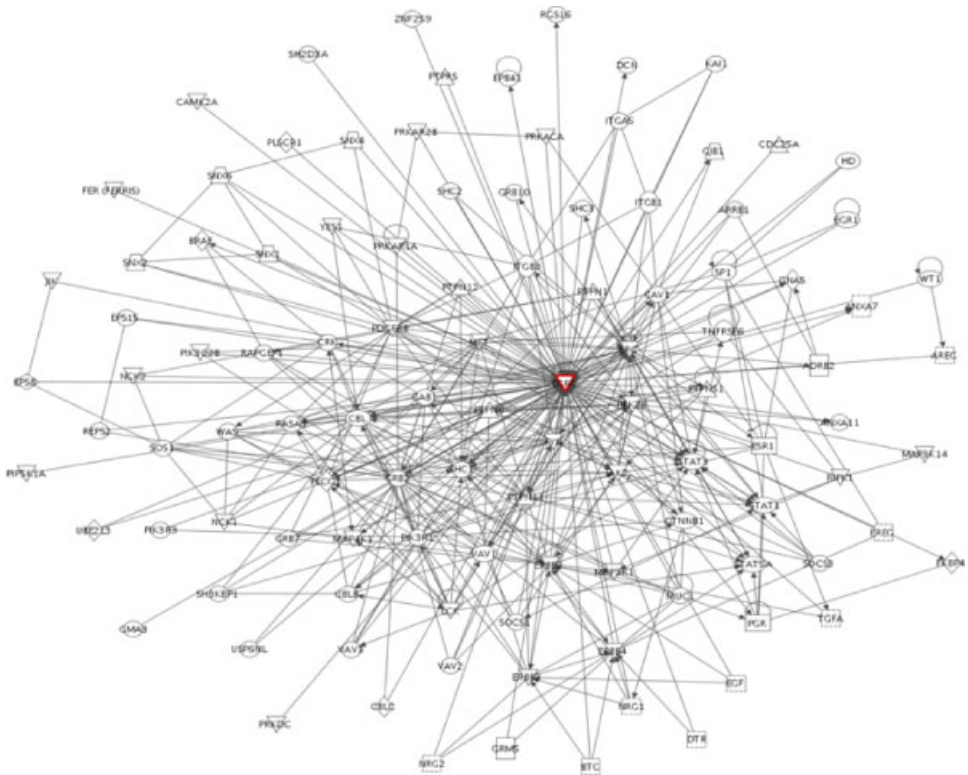

Fig. 5. Neighborhood proteins of EGFR indicating its complex regulatory relationships.

and VEGF (7), which indicates their potential cross-talk during the repair process.

Similar to the events occurring during intramembranous ossification, cell death has been once again identified as the most dominant functional theme during chondrogenesis. Upregulation of CASP14, KSR, MDM2 and downregulation of FADD, ITGB1, and SMAD4 are associated with survival signals while the significance of some other changes remains to be determined. Among the 12 potentially functioning pathways, PI3K/AKT signaling was the most statistically significant (seven differentially expressed proteins belong to this pathway). This pathway, which is considered to be important to mediate survival signals to cells, has not previously received substantial discussion in bone repair compared to other

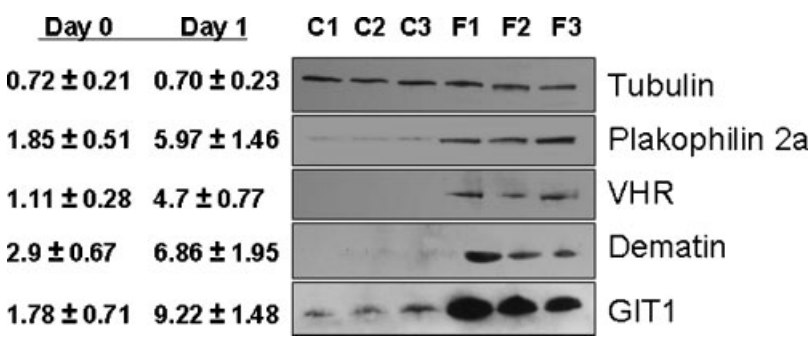

Fig. 6. Western blot analysis with normal and fractured bone on Day 1. Transferred filters were probed with Plakophilin 2a, VHR, Dematin, and GIT1 antibodies. C = normal; F = Fractured. All experiments were performed with three biological replicates. One control blot with Tubulin antibody was also included for loading control. Expression of all four#proteins was higher in fractured bone on Day 1 than normal controls that are consistent with the data derived from protein arrays. The numbers on the left side are normalized expression values derived from the protein arrays. Data are expressed as mean ± SD.

well-known pathways, such as those of PDGF and VEGF signaling. In this pathway, phosphatidylinositol (PI) 3-kinase (PI3K) is responsible for the recruitment of AKT to the plasma membrane, which is critical for AKT activation. Upregulation of PI3K (1.8-fold) could facilitate this recruitment process. Subsequent activation of AKT leads to phosphorylation and inactivation of proapoptotic molecules such as bad, forkhead, and caspase 9, and activation of molecules regulating cell growth and expression of genes responsible for survival [Datta et al., 1999]. Altogether, these data suggest that coordinated apoptotic death and cell proliferation signals are important mechanisms for promoting bone repair.

It is important to emphasize that more potentially active molecular pathways at chondrogenesis (Day 7) than any of the other four cellular events do not necessarily suggest that chondrogenesis itself is the most complicated process. Some of the active pathways observed at chondrogenesis may be involved in initiation of endochondral ossification. It has been previously observed that endochondral ossification is first seen on Day 9 in the same animal model as we used in this study [Jingushi et al., 1992]. Thus, it is not surprising that some of the endochondral ossification-related pathways are already active on Day 7.

On Day 14, the soft callus with less prominent neovasculature reduces its dimension to cover only near the vicinity of the fracture ends. Hypertrophic chondrocytes become the dominant cell type in the soft callus. Hematopoietic marrow formation is evident in the hard callus. Osteoclast-like cells of hemopoietic origin brought to the site by the revascularization of the bone ends remove the cartilage ECM and create a space in which osteoblasts are able to lay down significant amount of woven bone (approximately half of cartilage is replaced with bone on Day 14. Rosen and Thies, 1995; Einhorn, 1998). Corresponding to the transition of tissue types from chondrogenesis to endochondral ossification, which is involved in an ordered process of programmed cell death [Einhorn, 1998], we observed a molecular transition from proteins involved in cellular and molecular functions at chondrogenesis to those involved in physiological system development and functions at endochondral ossification on Day 14 (Fig. 4). Our data suggest that Day 14 is an active stage for the development of many physiological systems including hematological, immune, and lymphatic systems.

On Day 28, endochondral ossification ceases and repair enters the final and most prolonged cellular event of remodeling [Jingushi et al., 1992]. Hardcallus from both ends of fracture is joined by mature fibrous tissue with osteogenic and chondrogenic differentiations. Bone formation by osteoblasts is evident on the osteoclastic eroded surfaces of the dead cortical bone in the fracture ends. Pathway analysis identified integrin signaling as the most abundant (9 proteins) and significant ($P < 0.00002$) pathway at the remodeling stage. Integrins are primary sensors of the ECM environment. They recognize and bind to specific ECM ligands and transduce signals leading to the activation of intracellular signaling pathways, and the assembly/remodeling of actin-based adhesion complexes [Martin et al., 2002]. It has been shown that integrin signals generated during growth enhance the acquisition of a skeletal mass, structure, and strength to withstand mechanical loads [Globus et al., 2005]. Our data further support the significance of integrin signaling during the remodeling stage of bone repair. As a multi-functional signaling pathway, recent studies have also suggested that integrin-mediated adhesion can regulate cell survival [Damsky and Ilic, 2002]. One such example is signaling through integrin 1 to the PI3-kinase/Akt survival pathway, demonstrated by using fibroblasts cultured within three-dimensional collagen gels, a technique that mimics wound contraction [Tian et al., 2002]. PI3-kinase activity is highest during early stages of contraction, and then declines, resulting in apoptosis. Addition of an anti-integrin β1 antibody sustains elevated PI3-kinase activity, thereby blocking apoptosis and promoting cell survival. Thus, the downregulation of integrin β1 and upregulation of catalytic and regulatory subunits of PI3-kinase in our study support that this coordinated regulation is critical for promoting cell survival.

Because antibody arrays are a new technology for the study of fracture repair, it is important to understand their potential limitations. First, only a relatively small number of proteins are represented on the arrays and none of those is novel (i.e., all are existing and well-characterized proteins). Second, although many major cellular pathways such as signal transduction, apoptosis, cell cycle control, and

transcription are included, some other important pathways previously implicated in fracture repair are poorly represented, such as BMP and TGF-β families. Consequently, this analysis is biased toward well-characterized known proteins and the knowledge derived from this study is limited by the composition of the arrays. Further development of more comprehensive protein arrays are needed to reveal other signals important for fracture repair. In addition, we compared 84 differentially expressed proteins on Day 1 (Day 1 vs. Day 0) with their corresponding RNA expression at the same time point (Day 1 vs. Day 0), and found only 43 of the 84 genes (51%) differentially expressed in the same direction as their proteins (raw comparison data were published as supporting information at http://fgf.bsd.uchicago.edu/pickup/). Thus, it has to be cautious when one predicts protein expression based on RNA information.

In summary, genetic network analysis showed that many differentially expressed proteins at a given cellular event are functionally or physically correlated. Although most of these proteins are known, many of their actions have not been previously described during bone repair. At least 18 molecular pathways were potentially involved and 11 of these were active at more than one cellular event, indicating the complex and interdependent nature of the bone repair process. Regulation of cell cycle at inflammation seems a characteristic event for initiation of bone repair while control of cell death at the intramembranous ossification and chondrogenesis stages appear critical for cell proliferation. Uniquely activated integrin-signaling pathways during remodeling suggests its pivotal role in ensuring a quality finish of bone repair.

ACKNOWLEDGMENTS

We thank OrthoLogic Corp. for providing partial financial support, and Jeremiah Convery and Tammy Bigelow for performing animal surgery. We thank Subburaman Mohan from Loma Linda University and Mei-Shu Shih from Skeletech for the insightful discussion on cell types involved in fracture healing. We also thank Theodore Karrison from The University of Chicago for critical discussion on sample permutation. This work was also supported in part by the Division of Biological Sciences, the Cancer Research Center, and the NIDDK Biotechnology Center at the University of Chicago (U24D55370).

REFERENCES

Anderson K, Potter A, Baban D, Davies KE. 2003. Protein expression changes in spinal muscular atrophy revealed with a novel antibody array technology. Brain 126:2052–2064.

Bonnarens F, Einhorn TA. 1984. Production of a standard closed fracture in laboratory animal bone. J Orthop Res 2:97–101.

Bostrom MP, Asnis P. 1998. Transforming growth factor beta in fracture repair. Clin Orthop 355(Suppl):S124–S131.

Chen G, Gharib TG, Huang CC, Taylor JM, Misek DE, Kardia SL, Giordano TJ, Iannettoni MD, Orringer MB, Hanash SM, Beer DG. 2002. Discordant protein and mRNA expression in lung adenocarcinomas. Mol Cell Proteomics 1:304–313.

Cutler P. 2003. Protein arrays: The current state-of-the-art. Proteomics 3:3–18.

Damsky CH, Ilic D. 2002. Integrin signaling: It's where the action is. Cur Opin in Cell Biol 14:594–602.

Datta SR, Brunet A, Greenberg ME. 1999. Cellular survival: A play in three Akts. Genes Dev 13:2905–2927.

De Ceuninck F, Dassencourt L, Anract P. 2004. The inflammatory side of human chondrocytes unveiled by antibody microarrays. Biochem Biophys Res Commun 323:960–969.

Einhorn TA. 1998. The cell and molecular biology of fracture healing. Clin Orthop Rel Res 355S:S7–S21.

French DM, Kaul RJ, D'Souza AL, Crowley CW, Bao M, Frantz GD, Filvaroff EH, Desnoyers L. 2004. WISP-1 is an osteoblastic regulator expressed during skeletal development and fracture repair. Am J Pathol 165:855–867.

Ghobrial IM, McCormick DJ, Kaufmann SH, Leontovich AA, Loegering DA, Dai NT, Krajnik KL, Stenson MJ, Melhem MF, Novak AJ, Ansell SM, Witzig TE. 2005. Proteomic analysis of mantle cell lymphoma by protein microarray. Blood 105:3722–3730.

Globus RK, Amblard D, Nishimura Y, Iwaniec UT, Kim JB, Almeida EA, Damsky CD, Wronski TJ, van der Meulen MC. 2005. Skeletal phenotype of growing transgenic mice that express a function-perturbing form of beta1 integrin in osteoblasts. Calcif Tissue Int 76:39–49.

Haab BB. 2005. Antibody Arrays in Cancer Research. Mol Cell Proteomics 4:377–383.

Hadjiargyrou M, Lombardo F, Zhao S, Ahrens W, Joo J, Ahn H, Jurman M, White DW, Rubin CT. 2002. Transcriptional profiling of bone regeneration. J Biol Chem 277:30177–30182.

Hatano H, Siegel HJ, Yamagiwa H, Bronk JT, Turner RT, Bolander ME, Sarkar G. 2004. Identification of estrogen-regulated genes during fracture healing using DNA microarray. J Bone Miner Metab 22:224–235.

Hudelist G, Pacher-Zavisin M, Singer CF, Holper T, Kubista E, Schreiber M, Manavi M, Bilban M, Czerwenka Km. 2004. Use of high-throughput protein array for profiling of differentially expressed proteins in normal and malignant breast tissue. Breast Cancer Res Treat 86:281–291.

Hulth A. 1989. Current concepts of fracture healing. Clin Orthop Rel Res 249:265–284.

Jingushi S, Joyce ME, Bolander ME. 1992. Genetic expression of extracellular matrix proteins correlates with histologic changes during fracture repair. J Bone Miner Res 7:1045–1054.

Li C, Wong WH. 2001. Model-based analysis of oligonucleotide arrays: Expression index computation and outlier detection. Proc Natl Acad Sci USA 98:31–36.

Li X, Quigg RJ, Zhou J, Ryaby JT, Wang H. 2005. Early signals for fracture healing. J Cell Biochem 95:189–205.

Martin KH, Slack JK, Boerner SA, Martin CC, Parsons JT. 2002. Integrin connections map: To infinity and beyond. Science 296:1652–1653.

Mckibbin B. 1978. The biology of fracture healing in long bones. J Bone Joint Surgery 60B:150–162.

Nakazawa T, Nakajima A, Seki N, Okawa A, Kato M, Moriya H, Amizuka N, Einhorn TA, Yamazaki M. 2004. Gene expression of periostin in the early stage of fracture healing detected by cDNA microarray analysis. J Orthop Res 22:520–525.

Rosen V, Thies RS. 1995. The cellular and molecular basis of bone formation and repair. New York: Springer press.

Rosier RN, O'Keefe RJ, Hicks DG. 1998. The potential role of transforming growth factor beta in fracture healing. Clin Orthop 355(Suppl):S294–S300.

Tian B, Lessan K, Kahm J, Kleidon J, Henke C. 2002. β1 integrin regulates fibroblast viability during collagen matrix contraction through a phosphatidylinositol 3-kinase AKT/protein kinase B signaling pathway. J Biol Chem 277:24667–24675.